BI-TP 96/54
CERN-TH/96-334
HD-THEP-96-48
hep-lat/9612006
December 6, 1996

A NON-PERTURBATIVE ANALYSIS OF THE FINITE T PHASE TRANSITION IN SU(2)×U(1) ELECTROWEAK THEORY

K. Kajantie[a,b1], M. Laine[c2], K. Rummukainen[d3] and M. Shaposhnikov[a4]

[a] *Theory Division, CERN, CH-1211 Geneva 23, Switzerland*

[b] *Department of Physics, P.O.Box 9, 00014 University of Helsinki, Finland*

[c] *Institut für Theoretische Physik, Philosophenweg 16, D-69120 Heidelberg, Germany*

[d] *Fakultät für Physik, Postfach 100131, D-33501 Bielefeld, Germany*

Abstract

The continuum 3d SU(2)×U(1)+Higgs theory is an effective theory for a large class of 4d high-temperature gauge theories, including the minimal standard model and some of its supersymmetric extensions. We study the effects of the U(1) subgroup using lattice Monte Carlo techniques. When g'^2/g^2 is increased from the zero corresponding to pure SU(2)+Higgs theory, the phase transition gets stronger. However, the increase in the strength is close to what is expected perturbatively, and the qualitative features of the phase diagram remain the same as for $g'^2 = 0$. In particular, the first order transition still disappears for $m_H > m_{H,c}$. We measure the photon mass and mixing angle, and find that the mass vanishes in both phases within the statistical errors.

[1] keijo.kajantie@cern.ch
[2] m.laine@thphys.uni-heidelberg.de
[3] kari@physik.uni-bielefeld.de
[4] mshaposh@nxth04.cern.ch

1 Introduction

For reliable computations in the cosmology of the very early universe, it is indispensable to know the equation of state of the matter governed by the laws of the one correct – so far unknown – physical electroweak theory. For a large class of candidate theories an effective theory, the 3d SU(2)×U(1) + fundamental Higgs theory, can be derived by analytic perturbative computations [1, 2]. This effective theory gives an approximate but in many cases accurate description of the electroweak phase transition. The non-perturbative effects always encountered in a finite T context are isolated in the effective theory, which has to be solved numerically. Up to now, all non-perturbative efforts [3–8] were concentrated on an even simpler theory, without the U(1) factor. The 4d lattice simulations of the bosonic sector of the standard model [9] also do not take into account the U(1) group. (The present status of lattice Monte Carlo studies of the SU(2)+Higgs model both in the finite temperature 4d theory and in the 3d effective theory is reviewed in [10].) The purpose of this article is to complete the study by including the U(1) subgroup.

At first sight, the inclusion of the U(1) factor is harmless and may be done perturbatively. However, this need not be so in the vicinity of the phase transition. The dimensionless high-temperature expansion parameter associated with the U(1) group is $\sim g'^2 T/m$, where g' is the U(1) gauge coupling and m is a typical mass of a (hyper) charged particle in 3d. This parameter is indeed small deep in the broken phase (where m is the W boson mass, $m \sim gv$) and high in the symmetric phase (where m is the mass of a hypercharged scalar excitation, $m \sim gT$). However, near the critical temperature the scalar mass may be small and perturbation theory breaks down. Thus a Monte Carlo study is needed.

The inclusion of the U(1) factor also changes qualitatively the mass spectrum of the SU(2)+Higgs theory, as there is now an excitation (the photon) which is perturbatively massless in both phases. There are several interesting questions related to this excitation, for instance whether there might be non-perturbative mass generation for it and how the Weinberg mixing angle (defined in a suitable gauge independent manner) behaves in the vicinity of the phase transition.

It is important to keep in mind the separation of the two stages in the effective field theory approach. The first stage establishes the values of the parameters of the 3d effective theory in terms of the physical 4d parameters by means of a perturbative computation. This has already been done for the minimal standard model (MSM) in [1] and for the MSSM in [2]. The second stage is a non-perturbative lattice study of the 3d theory as such, performed in the present paper.

Since the simulations are rather demanding in computer time, we do not chart the entire critical surface but perform simulations only at two new points of the parameter space. The nonzero value of the U(1) gauge coupling $g_3'^2 = 0.3 g_3^2$ comes from the ratio of the physical values of m_W, m_Z in the minimal standard model. For the scalar

self-coupling we choose two values:

- $\lambda_3 = 0.06444 g_3^2$, which in the notation of [3] corresponds to $m_H^* = 60$ GeV (for the actual physical Higgs pole mass m_H in different 4d theories, see Sec. 3). This value of the "Higgs mass" was the most precisely studied case in the SU(2)+Higgs model. The first order nature of the phase transition here is clear.
- $\lambda_3 = 0.62402 g_3^2$, corresponding to $m_H^* = 180$ GeV. In the SU(2)+Higgs model first or second order phase transitions are absent then [4]. We find that the same statement is true when the U(1) interactions are added.

The paper is organized as follows. Sec. 2 is the formulation of the 3d problem in the continuum, Sec. 3 gives examples of 4d→3d connections and in Sec. 4 we describe how the theory is discretized. Some perturbative results are in Sec. 5. Sec. 6 contains the lattice results and a comparison with perturbation theory, and the conclusions are in Sec. 7.

2 Formulation of the problem in 3d

The Lagrangian of the effective theory (we keep only super-renormalizable interactions; the accuracy of this approximation in the MSM is discussed in [1, 11]) is:

$$L = \frac{1}{4} F_{ij}^a F_{ij}^a + \frac{1}{4} B_{ij} B_{ij} + (D_i \phi)^\dagger D_i \phi + m_3^2 \phi^\dagger \phi + \lambda_3 (\phi^\dagger \phi)^2, \tag{2.1}$$

where

$$\begin{aligned} F_{ij}^a &= \partial_i A_j^a - \partial_j A_i^a - g_3 \epsilon^{abc} A_i^b A_j^c \\ B_{ij} &= \partial_i B_j - \partial_j B_i \\ D_i &= \partial_i + i g_3 A_i + i g_3' B_i/2, \qquad A_i = \frac{1}{2} \sigma_a A_i^a, \\ \phi &= \begin{pmatrix} \phi_1 \\ \phi_2 \end{pmatrix} \equiv \begin{pmatrix} \phi^+ \\ \phi^0 \end{pmatrix}. \end{aligned} \tag{2.2}$$

The SU(2)×U(1) local gauge transformation is

$$\phi(x) \to e^{i\alpha(x)} G(x) \phi(x). \tag{2.3}$$

The four parameters of the theory, g_3^2, $g_3'^2$, λ_3 and m_3^2 are definite computable functions of the underlying 4d parameters and the temperature.

From the 3d point of view, the coupling constants g_3^2, $g_3'^2$ and λ_3 are renormalization group invariant, whereas the mass parameter m_3^2 gets renormalized at 2-loop level. In the $\overline{\rm MS}$ scheme, the renormalized part of m_3^2 is of the form

$$m_3^2(\mu) = \frac{f_{2m}}{16\pi^2} \log \frac{\Lambda_m}{\mu}, \tag{2.4}$$

where

$$f_{2m} = \frac{51}{16}g_3^4 - \frac{9}{8}g_3^2 g_3'^2 - \frac{5}{16}g_3'^4 + 9\lambda_3 g_3^2 + 3\lambda_3 g_3'^2 - 12\lambda_3^2, \tag{2.5}$$

and Λ_m is a constant specifying the theory.

All the four parameters of the 3d SU(2)×U(1)+Higgs theory are dimensionful. One may measure all the dimensionful observables in terms of one of the coupling constants, say g_3^2. The dynamics then depends on the three dimensionless parameters x, y and z, defined as

$$x \equiv \frac{\lambda_3}{g_3^2}, \qquad y \equiv \frac{m_3^2(g_3^2)}{g_3^4}, \qquad z \equiv \frac{g_3'^2}{g_3^2}. \tag{2.6}$$

These quantities are renormalization group invariant.

The question we are going to address is: "How does the phase structure and how do the gauge invariant operator expectation values depend on $z \geq 0$?" When $z = 0$ the U(1) interactions are decoupled and we get an SU(2)+Higgs theory, the phase structure of which has been studied in [3, 4]. In the opposite limit, $z \to \infty$ with x/z fixed, we get a 3d U(1)+Higgs model with global SU(2) symmetry. The physical value of z lies in between and is related to the Weinberg angle, $z \approx m_Z^2/m_W^2 - 1 \approx 0.3$.

The main characteristic of the 3d SU(2)+Higgs theory is the existence of a critical line $y = y_c(x)$ for $0 < x \leq x_c \approx 1/8$, along which the system has a first order transition. The transition gets weaker with increasing x and eventually terminates in a second order transition possibly of the Ising universality class at x_c. At $x > x_c$ there is no transition or a transition of higher than second order. If there is no transition, the two phases are analytically connected, which is possible since there is no local gauge invariant order parameter which would vanish in either of them [12–15]. The signal of the first order transition is that along $y = y_c(x)$ the system can coexist in two phases with different values of various gauge invariant operators like $\langle\phi^\dagger\phi\rangle$.

Correspondingly, for the SU(2)×U(1)+Higgs theory one expects that there is a critical surface $y = y_c(x, z)$, which for $z = 0$ coincides with the previous curve $y = y_c(x)$. For larger x the surface should terminate in a line of second order transitions, $x = x_c(z), x_c(0) \approx 1/8$ (Fig.1). Indeed, the statement about the non-existence of a local gauge invariant order parameter is unchanged. This expectation has to be confirmed numerically, and the precise magnitude of the effects of making $z > 0$ on various physical quantities have to be determined. Expressing everything in dimensionless form by scaling by powers of g_3^2, the quantities we are interested in are

- The critical curve $y = y_c(x, z)$,
- The jump $\Delta\ell_3$ of the order parameter like quantity $\ell_3 \equiv \langle\phi^\dagger\phi(g_3^2)\rangle/g_3^2$ between the broken and symmetric phases at y_c. In perturbation theory, $\Delta\ell_3 \sim \frac{1}{2}\phi_b^2(y_c)/g_3^2$, where ϕ_b is the location of the broken minimum in, say, the Landau gauge,

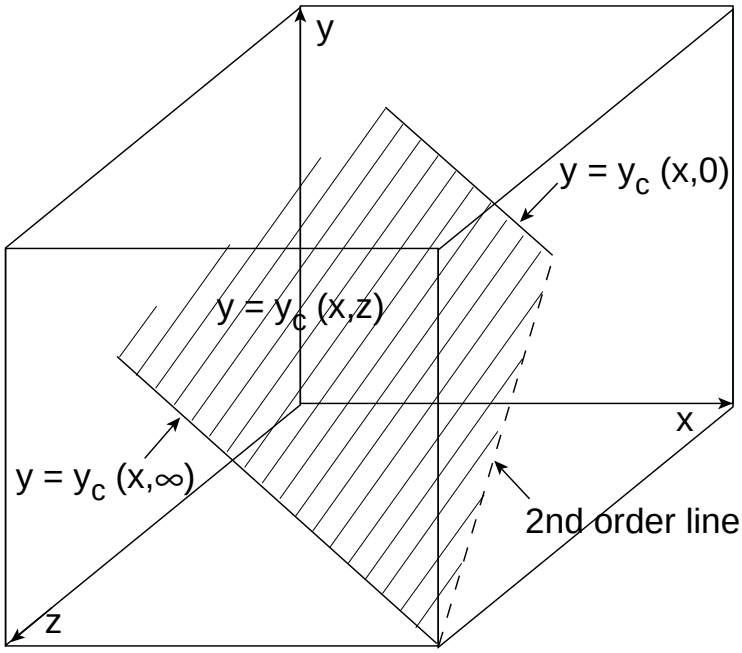

Figure 1: The expected schematic phase diagram of the SU(2)×U(1)+Higgs theory in the space of the parameters of eq.(2.6). There is a 1st order transition which terminates in a line of 2nd order transitions.

- The interface tension σ_3, defined in perturbation theory by

$$\sigma_3 = \int_0^{\phi_b/g_3} d(\phi/g_3)\sqrt{2V(\phi/g_3)/g_3^6}. \tag{2.7}$$

A non-perturbative study of the dynamics of the theory is based on a study of the expectation values and correlators of low-dimensional gauge invariant operators, so for completeness we will review these here. It is convenient to introduce a matrix parametrisation of the Higgs field by writing

$$\Phi = \left((\tilde{\phi})(\phi)\right) \equiv \begin{pmatrix} \phi_2^* & \phi_1 \\ -\phi_1^* & \phi_2 \end{pmatrix}. \tag{2.8}$$

Under an SU(2)×U(1) gauge transformation Φ transforms according to

$$\Phi(x) \to G(x)\Phi e^{-i\alpha(x)\sigma_3}. \tag{2.9}$$

The global transformation

$$\Phi(x) \to \Phi(x)C^{-1} \tag{2.10}$$

where C is an SU(2) matrix, will be seen to be an isospin custodial rotation of the vector states W_i^a.

In order of increasing dimensionality the list of gauge-invariant operators is:

- Dim = 1: $\phi^\dagger\phi$. Note that $\tilde{\phi}^\dagger\phi = 0$; there is only one singlet.
- Dim = 3/2: B_{ij}, the U(1) field.
- Dim = 2: there are two independent gauge invariant operators, namely a vector $\phi^\dagger D_i\phi - (D_i\phi)^\dagger\phi$ and a scalar $(\phi^\dagger\phi)^2$. For the SU(2)+Higgs case ($z = 0$) there are two extra vector operators. In terms of the matrix representation (2.8) the vector operators invariant under the SU(2) subgroup are

$$\begin{aligned} W_i^a &= i\mathrm{Tr}\,\Phi^\dagger D_i\Phi\sigma_a \\ &= \frac{1}{2}i\mathrm{Tr}\,[\Phi^\dagger D_i\Phi - (D_i\Phi)^\dagger\Phi]\sigma_a. \end{aligned} \tag{2.11}$$

  Under the U(1) gauge transformation (2.9) (which is a rotation around the 3-axis in isospace)

$$W_i^a \to i\mathrm{Tr}\,\Phi^\dagger D_i\Phi(e^{-i\theta\sigma_3}\sigma_a e^{i\theta\sigma_3}), \tag{2.12}$$

  so that $W_i^{1,2}$ are not gauge-invariant but W_i^3 is. Note that

$$\mathrm{Tr}\,[\Phi^\dagger D_i\Phi + (D_i\Phi)^\dagger\Phi] = 2\partial_i(\phi^\dagger\phi) \tag{2.13}$$

  and does not bring in anything new. We remark also that in the SU(2)×U(1) theory the custodial symmetry is explicitly broken. Under the custodial transformation (2.10) the operators in (2.11) transform as vectors in the space of $a = 1, 2, 3$,

$$W_i^a \to i\mathrm{Tr}\,\Phi^\dagger D_i\Phi C^{-1}\sigma_a C, \tag{2.14}$$

  and thus a mixing of gauge-invariant and gauge-noninvariant operators occurs.
- Dim = 5/2: $\phi^\dagger F_{ij}\phi$, $\phi^\dagger\phi B_{ij}$.
- Dim = 3: Terms in the action.
- Dim = 7/2: The parity violating $J^{PC} = 0^{-+}$ terms

$$P_1 = i\epsilon_{ijk}[\phi^\dagger D_k\phi - (D_k\phi)^\dagger\phi]B_{ij}, \tag{2.15}$$

$$P_2 = i\epsilon_{ijk}[\phi^\dagger F_{ij}D_k\phi - (D_k\phi)^\dagger F_{ij}\phi]. \tag{2.16}$$

  The list of parity odd operators can be extended by two non-local operators,

$$e^{i2\pi N_{\mathrm{CS}}}, \tag{2.17}$$

where

$$N_{\rm CS2} = \frac{g^2}{16\pi^2}\int d^3x\,\epsilon_{ijk}{\rm Tr}\left(A_iF_{jk} - \frac{2}{3}igA_iA_jA_k\right) \tag{2.18}$$

and

$$N_{\rm CS1} = \frac{g'^2}{16\pi^2}\int d^3x\,\epsilon_{ijk}B_iB_{jk}. \tag{2.19}$$

In this paper we mainly use the scalar operator $\phi^\dagger\phi$, the U(1) operator B_{ij} and the vector operator W_i^3.

3 4d $\to$ 3d relation

As emphasized earlier, it is important to separate the two stages of solving the finite T problem: relating the 4d and 3d theories and discussing the 3d theory as such. The mapping here is many $\to$ few; many different 4d theories with different parameter values can correspond to a single set of 3d parameters x, z. This has to be worked out for each case separately and here we only give a couple of examples for illustration.

Firstly and most qualitatively, assume that we have an SU(2)×U(1) theory without fermions. Using tree-level relations between physics and couplings and integrating out A_0, gives a simple analytic relation (eqs.(2.8-10) of [3]). According to that relation, $x = 0.06444, 0.62402$ correspond to $m_H^* = 60, 180$ GeV and $z = 0, 0.3$ correspond to $m_Z = m_W, m_Z^{\rm exp}$.

Secondly, take the minimal standard model and the 1-loop equations relating x, y, z to physical parameters as given in [1]. Then $x = 0.06444$ corresponds to $m_H = 51.2$ GeV and $x = 0.62402$ to $m_H = 174$ GeV. The value of $z = z_c$ at T_c for given $m_H, m_{\rm top}$ is given in Fig. 2. Since z_c depends only logarithmically on T, we have estimated T_c from $y = 0$ (the true y_c is very close to zero, see below).

As a third example, take the minimal supersymmetric standard model. Fig. 3 shows different sets of values of the lightest Higgs mass m_H, the right-handed stop mass $m_{\tilde{t}_R}$ and the CP-odd Higgs mass m_A which all lead to the same value $x = 0.06444$.

4 The lattice-continuum relations

The lattice action corresponding to the continuum theory (2.1) is

$$\begin{aligned} S &= \beta_G\sum_x\sum_{i<j}[1 - \frac{1}{2}{\rm Tr}\,P_{ij}] \\ &+ \beta'_G\sum_x\sum_{i<j}[1 - \frac{1}{2}(p_{ij}^{1/\gamma} + p_{ij}^{*1/\gamma})] \end{aligned}$$

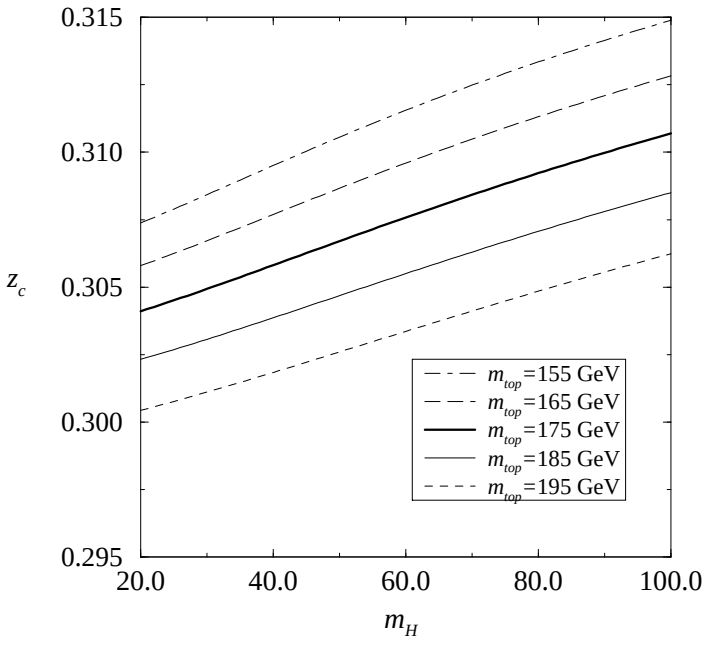

Figure 2: The value of $z = g_3'^2/g_3^2 = z_c$ at $T = T_c$ as a function of the physical Higgs mass m_H and the top quark mass $m_{\rm top}$ for the minimal standard model. The dependence shown arises mainly from the dependence of m_W on m_H, $m_{\rm top}$ (see [1] for the formulas used), and gives an estimate of the uncertainty in the physical value of z_c. The value of T_c is computed from $m_3^2(g_3^2) = 0$; the dependence of z_c on T_c is only logarithmic.

$$
\begin{aligned}
- \quad & \beta_H \sum_x \sum_i \frac{1}{2} \mathrm{Tr}\, \Phi^\dagger(x) U_i(x) \Phi(x+i) e^{-i\alpha_i(x)\sigma_3} \\
+ \quad & \sum_x (1 - 2\beta_R) \frac{1}{2} \mathrm{Tr}\, \Phi^\dagger(x)\Phi(x) + \beta_R \sum_x [\frac{1}{2} \mathrm{Tr}\, \Phi^\dagger(x)\Phi(x)]^2 . \qquad (4.1)
\end{aligned}
$$

Here the SU(2) and U(1) plaquettes are

$$
\begin{aligned}
P_{ij}(x) &= U_i(x) U_j(x+i) U_i^\dagger(x+j) U_j^\dagger(x), \qquad (4.2) \\
p_{ij}(x) &= \exp\{ i[\alpha_i(x) + \alpha_j(x+i) - \alpha_i(x+j) - \alpha_j(x)] \}. \qquad (4.3)
\end{aligned}
$$

Any positive number γ gives the same naive continuum limit, but if $\exp(-i\alpha_i(x)\sigma_3)$, $p_{ij}^{1/\gamma}$ are to be representations of the U(1) group and $\alpha \in (0, 2\pi)$, then one has to choose $\gamma = 1, 1/2, 1/3, \ldots$. The topological effects associated with $\gamma \neq 1$ vanish in the continuum limit.

A crucially important relation is the one expressing the four dimensionless lattice parameters β_G, β_G', β_H, β_R of eq. (4.1) in terms of the four dimensionless continuum parameters $g_3^2 a, x, y, z$. This relation, which can be derived using the techniques in [16],

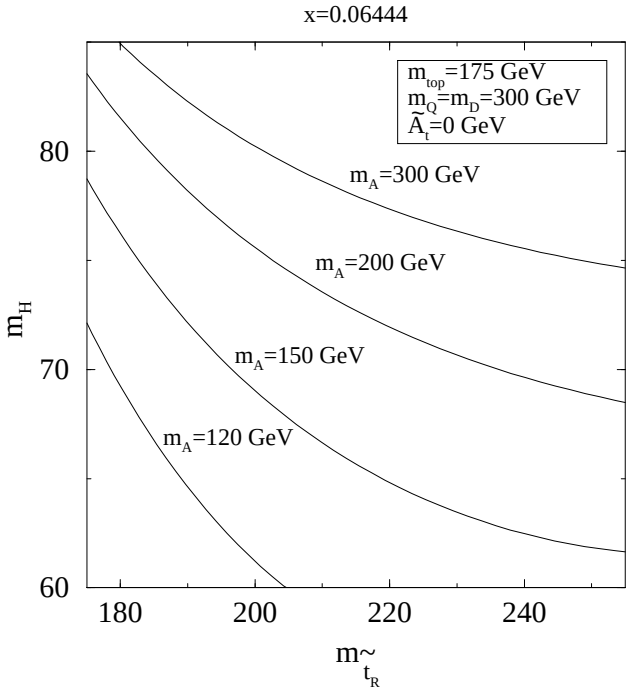

Figure 3: Examples of parameter values corresponding to $x = 0.06444$ in the MSSM. Here $m_{\tilde{t}_R}$ is the right-handed stop mass, m_H is the lightest CP-even Higgs mass and m_A is the CP-odd Higgs mass. The squark mixing parameters have been put to zero.

is

$$g_3^2 a = \frac{4}{\beta_G}, \tag{4.4}$$

$$x = \frac{\beta_R \beta_G}{\beta_H^2}, \tag{4.5}$$

$$z = \gamma^2 \frac{\beta_G}{\beta'_G}, \tag{4.6}$$

$$\begin{aligned} y = {} & \frac{\beta_G^2}{8\beta_H}(1 - 2\beta_R - 3\beta_H) + \frac{\Sigma\beta_G}{32\pi}(3 + 12x + z) \\ & + \frac{1}{16\pi^2}\Big[\Big(\frac{51}{16} - \frac{9}{8}z - \frac{5}{16}z^2 + 9x - 12x^2 + 3xz\Big)\Big(\ln\frac{3}{2}\beta_G + 0.09\Big) \\ & + 5.0 - 0.9z + \Big(0.01 + \frac{1.7}{\gamma^2}\Big)z^2 + 5.2x + 1.7xz\Big], \end{aligned} \tag{4.7}$$

where $\Sigma = 3.17591$. This relation is exact in the limit $a \to 0$. In [17] it was further proposed (for $\gamma = 1$) that the 1-loop $O(a)$-corrections could be removed by modifying (4.4)–(4.6) with terms of relative magnitude $O(1/\beta_G)$.

In usual discretisations of the U(1) gauge theory, $\gamma = 1$. In the physical situation the parameter z (eq.(2.6)) is about 0.3 and then the lattice coupling $\beta'_G = \beta_G/z$ (eq.(4.6)) would be rather large when approaching the continuum limit $\beta_G \to \infty$. Using a value $\gamma < 1$ permits one to have a smaller value of β'_G which makes finite size effects

smaller; the price one pays is an increasing correction term in eq.(4.7) and larger $O(a)$-corrections related to $g_3'^2$.

The historical motivation for the form (4.1) of the lattice action was to permit one to go to the fixed length limit of the Higgs field by taking $\beta_R \to \infty$. This limit is irrelevant now and it is actually possible very simply to combine (4.1) and (4.4)–(4.7) by rescaling the Higgs field so that the coefficient of the quartic term is +1. The lattice action for fixed a and fixed continuum variables g_3^2, x, y, z then is

$$\begin{aligned} S &= \beta_G \sum_x \sum_{i<j} [1 - \frac{1}{2}\mathrm{Tr}\, P_{ij}] \\ &+ \beta'_G \sum_x \sum_{i<j} [1 - \frac{1}{2}(p_{ij}^{1/\gamma} + p_{ij}^{*1/\gamma})] \\ &- \sqrt{\frac{\beta_G}{x}} \sum_x \sum_i \frac{1}{2}\mathrm{Tr}\, \Phi^\dagger(x) U_i(x) \Phi(x+i) e^{-i\alpha_i(x)\sigma_3} \\ &+ \sqrt{\frac{\beta_G}{x}} \Big\{ 3 + \frac{8}{\beta_G^2} y - \frac{\Sigma(3+12x+z)}{4\pi\beta_G} - \frac{1}{2\pi^2\beta_G^2}\Big[\ldots\Big] \Big\} \sum_x \frac{1}{2}\mathrm{Tr}\, \Phi^\dagger(x)\Phi(x) \\ &+ \sum_x [\frac{1}{2}\mathrm{Tr}\, \Phi^\dagger(x)\Phi(x)]^2, \end{aligned} \tag{4.8}$$

where the square bracket is the same as in (4.7).

Finally, in the continuum limit, the relation of the gauge-invariant lattice observable $\langle \frac{1}{2}\mathrm{Tr}\, \Phi^\dagger\Phi \rangle$ in (4.1) to the renormalized gauge-invariant continuum quantity $\langle \phi^\dagger\phi(\mu) \rangle$ in the $\overline{\mathrm{MS}}$ scheme is

$$\frac{\langle \phi^\dagger\phi(\mu) \rangle}{g_3^2} = \frac{\beta_G\beta_H}{8} \Big\langle \frac{1}{2}\mathrm{Tr}\, \Phi^\dagger\Phi \Big\rangle - \frac{\Sigma\beta_G}{8\pi} - \frac{1}{16\pi^2}(3+z)\Big(\log\frac{3\beta_G g_3^2}{2\mu} + 0.67\Big). \tag{4.9}$$

The 1-loop $O(a)$ corrections to the discontinuity of $\langle \phi^\dagger\phi(\mu) \rangle$ were also computed in [17].

5 Perturbative results

For understanding the magnitude of the expected effect of the U(1) subgroup, it is useful to compute it in perturbation theory. We have done this for the quantities listed in Section 2: the critical curve $y = y_c(x,z)$, the jump $\Delta\ell_3$ of the order parameter $\ell_3 \equiv \langle \phi^\dagger\phi(g_3^2) \rangle / g_3^2$ between the broken (b) and symmetric (s) phases at y_c and the interface tension σ_3.

The coarsest approximation, which nevertheless gives the general pattern and can be given in analytic form, is obtained by taking the 1-loop potential and including only the vector loops. The result then is

$$y_c(x,z) \;=\; \frac{1}{128\pi^2 x}\Big[\frac{2}{3} + \frac{1}{3}(1+z)^{3/2}\Big]^2,$$

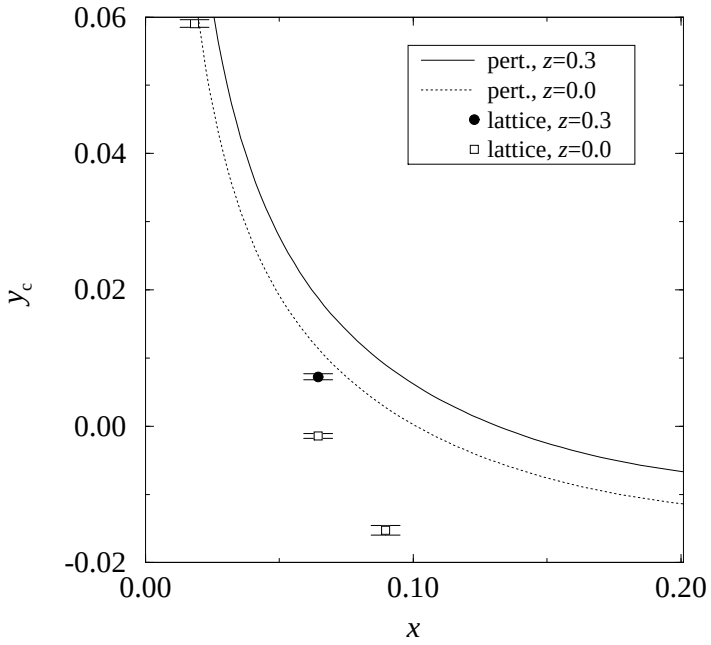

Figure 4: The curves show the values of $y_c(x,z)$ computed from the 3d 2-loop effective potential of the SU(2)×U(1)+Higgs model. Lattice Monte Carlo results are also shown. The perturbative curves continue to large values of x, but on the lattice the first order transition ends at $x \sim 1/8$. Beyond that in the cross-over region, the values obtained for $z = 0$ with the $\max(\chi_{R^2})$-method (see Sec. 6.1) are $y_c(0.274, 0) = -0.066$, $y_c(0.624, 0) = -0.16$.

$$\begin{aligned} \Delta\ell_3 &= \frac{1}{128\pi^2 x^2}\left[\frac{2}{3} + \frac{1}{3}(1+z)^{3/2}\right]^2, \\ \sigma_3 &= \frac{1}{6(16\pi)^3}\left(\frac{2}{x}\right)^{5/2}\left[\frac{2}{3} + \frac{1}{3}(1+z)^{3/2}\right]^3. \end{aligned} \tag{5.1}$$

Here one sees concretely how increasing z increases the quantities studied.

A more accurate result is obtained with 2-loop optimised 3d perturbation theory. The effective potential for the 3d SU(2)+Higgs theory is given and its optimisation is discussed in [18]. Since the effects of $g_3'^2$ are very small, it is sufficient for the present purpose to differentiate between m_W^2 and m_Z^2 only at 1-loop level (the complete 2-loop potential can be inferred from the 4d results in [19, 20]). A numerical computation then leads to the results shown in Figs. 4, 5. The figures also give the results from lattice Monte Carlo simulations [3, 4] and make it clear how the perturbative discussion is a good qualitative quide, but fails in a crucial property of the transition: its termination.

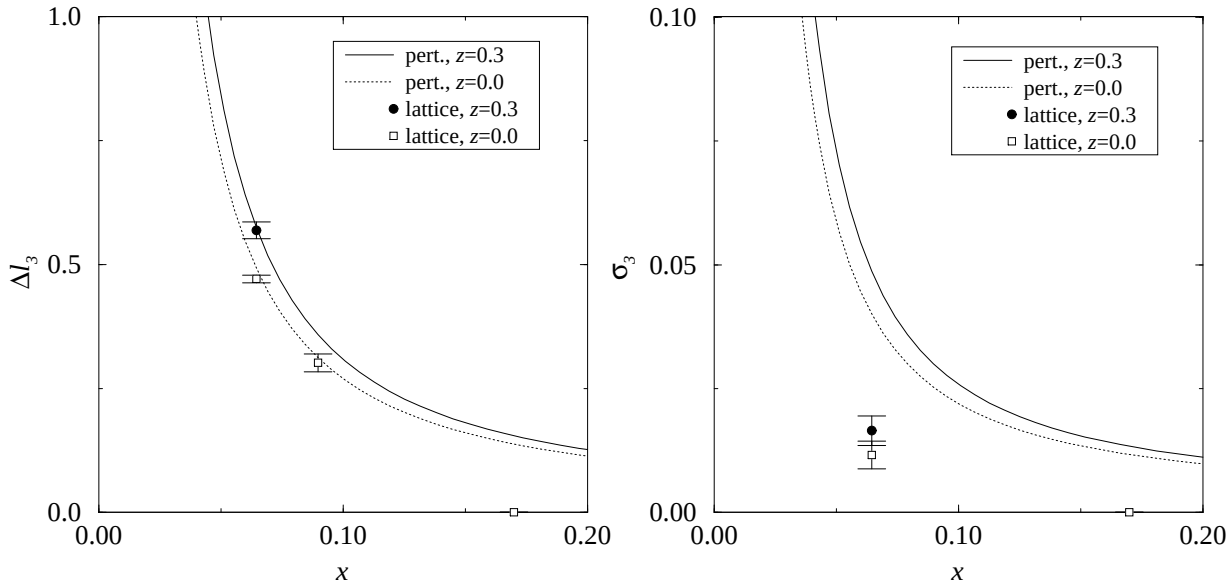

Figure 5: The same as Fig. 4 but for the jump of the order parameter and the interface tension. At $x \approx 0.096$, the interface tension was estimated in [6] to be $\sigma_3 \sim 1 \times 10^{-3}$. For $x \gtrsim 1/8$, there is no transition and $\Delta\ell_3$, σ_3 vanish.

6 Simulations

The simulations with the SU(2)×U(1)+Higgs action (4.1) are rather similar to those for the SU(2)+Higgs theory, described in detail in [3]. We shall, therefore, mainly just present the results and compare them. We have performed simulations with $x = 0.06444$ and $x = 0.62402$. For the SU(2)+Higgs case the former value gives a clear first order transition, whereas for the latter value the transition becomes a regular cross-over [3, 4]. Since the most precise results for the SU(2)+Higgs theory were for $x = 0.06444$ we shall concentrate mostly on this x-value. For z we always take $z = 0.3$.

The simulations were mainly performed on a Cray C-90 supercomputer at the Center for Scientific Computing, Finland. Some of the smaller volume simulations were done on workstation clusters. The total amount of computing power used for the $z = 0.3$ case was about 4.5 Cray cpu-months, or 2.3×10^{15} floating point operations, to be compared with 5×10^{15} flop for $z = 0$.

6.1 The transition point $y = y_c(x = 0.06444, z = 0.3)$

Let us first discuss the $x = 0.06444$ case, where the transition is relatively strongly first order ($m_H^* = 60\,\mathrm{GeV}$ in the notation used in [3]). The SU(2)×U(1)+Higgs model does not have a local gauge invariant order parameter. We identify the transition by

studying order parameter like quantities, $R^2 \equiv \sum_x R^2(x)/\mathrm{Vol}$ and

$$L \equiv \frac{1}{3\mathrm{Vol}} \sum_{x,i} \frac{1}{2} \mathrm{Tr}\, V^\dagger(x) U_i(x) V(x+i) e^{-i\alpha_i(x)\sigma_3}\,, \tag{6.1}$$

where V is the SU(2)-direction of the Higgs field: $\Phi = RV$. These operators develop a discontinuity at the transition point, as shown by the probability distributions $p(R^2)$ in Fig. 6 for $\beta_G = 5$ and 8. The development of a strong two-peak structure with an increasing volume is unambiguous.

In order to obtain the physical value of $y_c(x,z)$ we have to treat the finite volume effects and finite lattice spacing effects systematically. Our procedure here consists of the following stages:

The pseudocritical coupling. For fixed x and β_G (lattice spacing) and each lattice size we determine the pseudotransition coupling $\beta_{H,c}$ by several methods:

(1) maximum location of the R^2-susceptibility $\chi_{R^2} = \langle (R^2 - \langle R^2 \rangle)^2 \rangle$,
(2) minimum location of the Binder cumulant $B_L = 1 - \langle L^4 \rangle / (3 \langle L^2 \rangle^2)$,
(3) "equal weight" β_H-value for the distribution $p(R^2)$,
(4) "equal height" β_H-value for $p(L)$.

In practice, we perform a series of simulations with different values of β_H for fixed β_G and x (implying *not* fixed β_R but given by eq.(4.5)) until we have a good coverage of the transition region. The β_H-values corresponding to the above criteria are then found with the Ferrenberg-Swendsen multihistogram reweighting [21], and the error analysis is performed with the jackknife method. For all but the smallest volumes it is necessary to use multicanonical simulations [22]. For technical details we refer to [3], where a similar analysis was carried out for the SU(2)+Higgs model.

x	β_G	γ	volumes
0.06444	5	1	$8^2 \times 32_m$ $10^2 \times 40_m$ $12^2 \times 42_m$ $14^2 \times 56_m$
	8	1	24^3_m 32^3_m $16^2 \times 112_m$ $20^2 \times 120_m$ $24^2 \times 120_m$ $28^2 \times 112_m$
	16	1/2	12^3 16^3 24^3 32^3 $24^2 \times 72_m$ $32^2 \times 96_m$ $40^2 \times 120_m$
0.62402	8	1	12^3 16^3 24^3 32^3

Table 1: The lattice sizes used for the simulations at the transition temperature for each (x, β_G)-pair. In most of the cases, several β_H-values were used around the transition point. Multicanonical simulations are marked with the subscript $(_m)$.

The lattice volumes used in the simulations are listed in Table 1. For $x = 0.06444$ we used β_G values 5, 8 and 16; in the last case we used $\gamma = 1/2$ in order to avoid too large finite size effects.

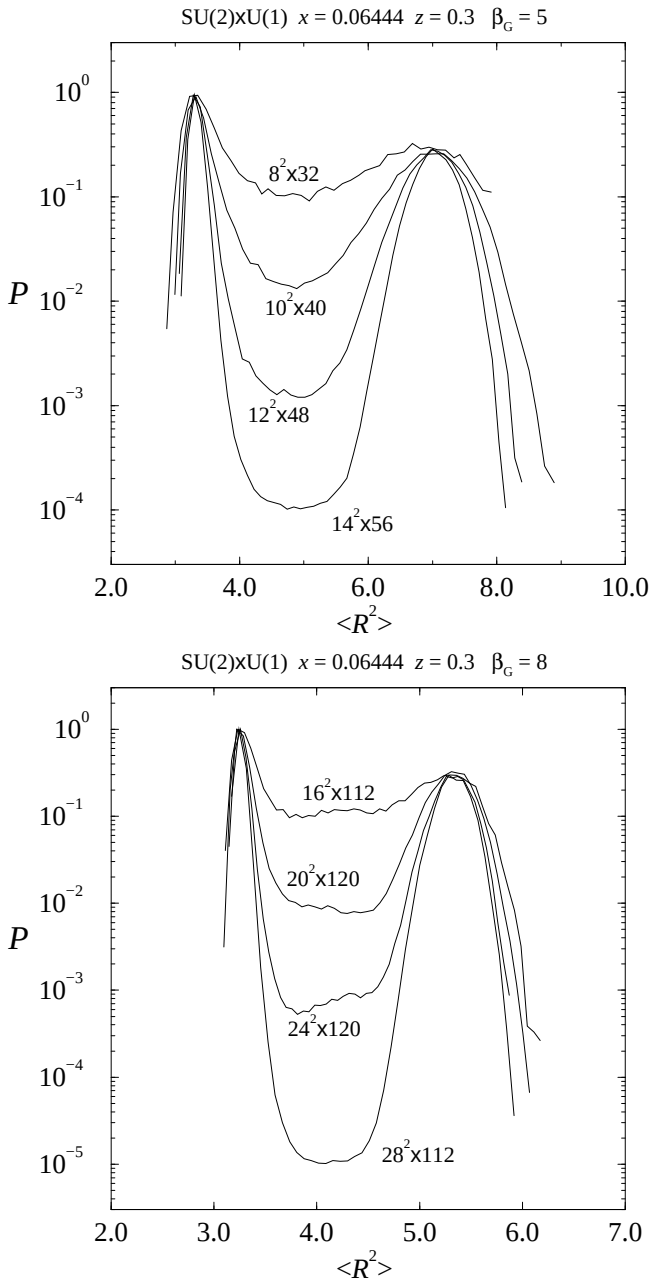

Figure 6: The "equal weight" distributions of the average Higgs length squared $R^2 = \sum_x R^2(x)/V$ at the transition point for $\beta_G = 5$ (upper) and 8 (lower) for $x = 0.06444$.

The infinite volume limit. For any given lattice, the criteria (1)–(4) above yield different values for the pseudocritical coupling $\beta_{H,c}$. However, in the thermodynamic limit $V \to \infty$, all the methods extrapolate very accurately to the same value, as shown in Fig. 7. It should be noted that the different methods do not yield statistically independent results, and combining the results together is not justified. In the extra-

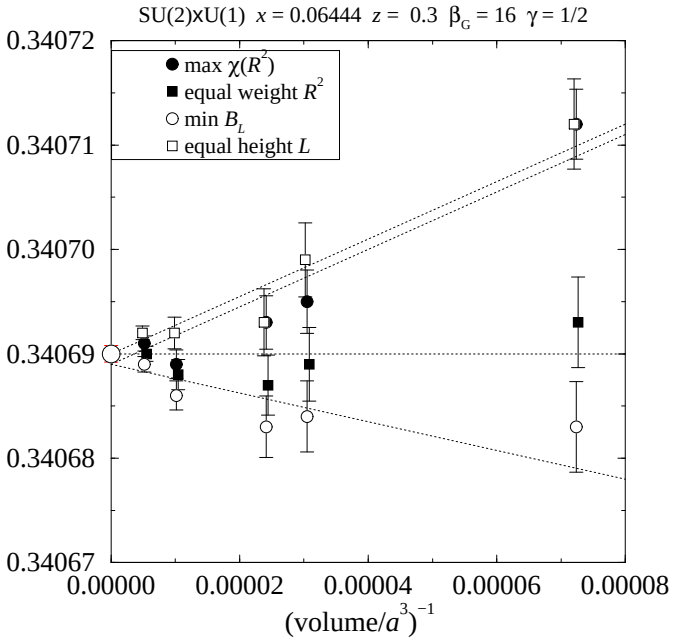

Figure 7: The $V = \infty$ limit of the pseudocritical couplings $\beta_{H,c}$ for $x = 0.06444$ ($m_H^* = 60$ GeV) and $\beta_G = 16$, calculated with four different methods. The figures for $\beta_G = 5, 8$ are similar.

β_G	γ	$\beta_{H,c}$	y_c
5	1	0.359863(3)	0.00199(7)
8	1	0.3489001(11)	0.00255(7)
16	1/2	0.3406899(8)	0.00489(20)
∞		1/3	0.0072(5)

Table 2: The infinite volume critical couplings $\beta_{H,c}$ and the associated values of y_c at $x = 0.06444$, $z = 0.3$ (from eq.(4.7)). The values of $\beta_{H,c}$ are calculated from the "equal weight of $p(R^2)$" data.

polations we used only volumes which are large enough in order to be compatible with the linear behaviour in $1/V$. In Table 2 we give the results using the "equal weight" values of the $p(R^2)$ distributions. Also shown are the corresponding values of y_c, obtained through eq. (4.7). Note that the value $\gamma = 1/2$ for $\beta_G = 16$ enters only through a 2-loop contribution in eq. (4.7); nevertheless, its inclusion is numerically crucial.

The continuum limit. Lastly, the physical value of y_c is obtained by extrapolating the $y_c(x, z; \beta_G)$ values to zero lattice spacing ($\beta_G = 4/(g_3^2 a) \to \infty$). This is shown in Fig. 8. The leading behaviour is linear in a; however, it is clearly impossible to fit a straight line through all β_G-values. In principle, the finite a curve is *different* for each

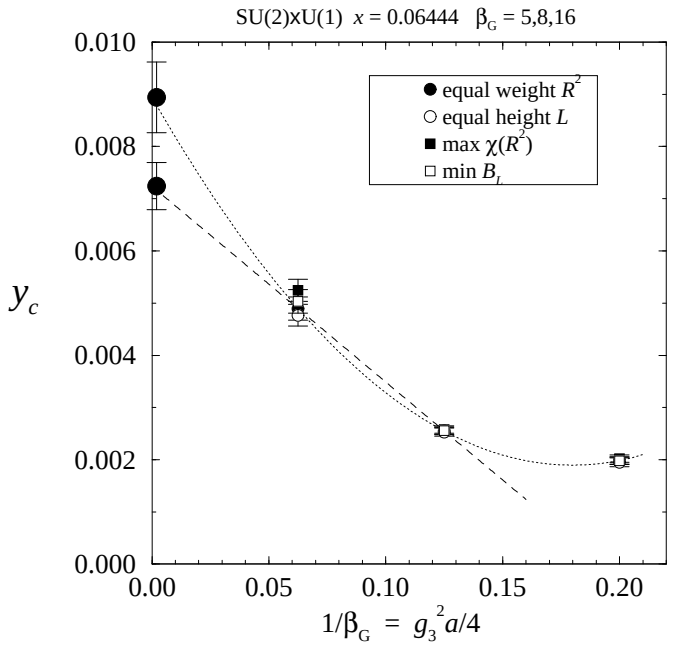

Figure 8: The continuum limit ($\beta_G \to \infty$) of the critical temperature for $x = 0.06444$ ($m_H^* = 60$ GeV), $z = 0.3$.

value of γ, and fitting an extrapolation through $\beta_G = 5$ and 8 ($\gamma = 1$) and $\beta_G = 16$ ($\gamma = 1/2$) datapoints is not rigorously justified. Nevertheless, when we compare this curve with the SU(2)+Higgs one (Fig. 11 in [3]), the qualitative similarity is obvious. However, the curvature of the quadratic fit is here clearly larger, and at $\beta_G = 5$ the quadratic fit already starts to turn upwards. We assume that this behaviour is not physical and that the quadratic extrapolation overestimates the continuum value of y_c. Therefore, in Table 2 we quote the value extrapolated linearly from $\beta_G = 8$ and $\beta_G = 16$ -points; however, the difference between the linearly and quadratically extrapolated values is small and does not affect our conclusions.

In Table 3 we compare the Monte Carlo results with the perturbative values. It is seen that for $\Delta\ell_3$ and σ_3 (whose determination is discussed below) the effect of z is just what is expected from the dominant 1-loop perturbative effect of $g_3'^2$. For y_c the discrepancy is slightly larger; however, here the lattice determination of y_c is not that easy (as explained in the previous paragraph). In any case the difference is small, and in terms of the critical temperature T_c the discrepancy is below 1% since y_c is composed of m_H^2 and $g^2 T_c^2$ as a difference of two large terms. Thus for any physical conclusions, we can say that the last block in Table 10 of [3], which was based on a purely perturbative estimate of the effects of the U(1) group, can be considered reliable.

measured	$z = 0$	$z = 0.3$	expected if U(1) perturbative
$y_c^{\rm latt}$	-0.00142(36)	0.00724(45)	0.0060
$y_c^{\text{2-loop}}$	0.01141	0.01882	
$\Delta\ell_3^{\rm latt}$	0.471(8)	0.569(17)	0.55
$\Delta\ell_3^{\text{2-loop}}$	0.493	0.575	
$\sigma_3^{\rm latt}$	0.0116(28)	0.0165(30)	0.014
$\sigma_3^{\text{2-loop}}$	0.0401	0.0487	

Table 3: Comparison of measured values and expected values at $x = 0.06444, z = 0.3$ if the effect of U(1) is perturbative. The 'expected' values are obtained by computing the difference (y_c) or ratio ($\Delta\ell_3$, σ_3) of the lattice and perturbative values at $z = 0$, and by using these numbers in modifying the perturbative values for $z = 0.3$. Note that the $z = 0$ values are slightly different from those in Table 10 of [3], since there the extrapolation to the continuum limit was made using the 4d observables T_c^*, L/T_c^{*4}, σ/T_c^{*3} whereas here we use directly the 3d observables.

6.2 The interface tension and $\Delta\langle\phi^\dagger\phi\rangle$

We measure the interface tension with the histogram method [23]. At the transition point the probability of the two bulk phases is equal, but a system of a finite volume can also exist in a mixed state consisting of domains of the two bulk phases. The probability of the mixed state is suppressed by the free energy of the interface between the bulk phases. As a result, an order parameter distribution develops a characteristic 2-peak structure (Fig. 6), and the interface tension σ_3 can be extracted from the limit

$$\sigma_3 = \lim_{V\to\infty} \frac{1}{2g_3^4 A} \ln \frac{P_{\rm max}}{P_{\rm min}}, \tag{6.2}$$

where $P_{\rm max}$ and $P_{\rm min}$ are the values of the distribution at the peak and at the plateau between the peaks, and A is the smallest cross-sectional area on a three-dimensional periodic volume. In practice a careful finite size analysis is required; for technical details we again refer to the discussion in [3].

The extrapolation of σ_3 to the infinite volume for each lattice spacing is shown in the upper part of Fig. 9 and to the continuum limit $a = 0$ in the bottom part. The final result is shown in Table 3 together with the perturbative estimates.

Let us next consider the measurements of the discontinuity of the condensate $\langle\phi^\dagger\phi\rangle$. The lattice quantities $R^2 \equiv \frac{1}{2}{\rm Tr}\,\Phi^\dagger\Phi$ are first converted to the values of the continuum condensate at scale g_3^2 by using eq. (4.9): $\ell_3 \equiv \langle\phi^\dagger\phi(g_3^2)\rangle/g_3^2$. The $\Delta\langle R^2\rangle$ discontinuity is extracted from the "equal weight" distributions $p(R^2)$ by measuring the positions of the peaks. The peak positions are determined by fitting parabolas to the distributions near the peaks. For each value of β_G the measurements are extrapolated to infinite

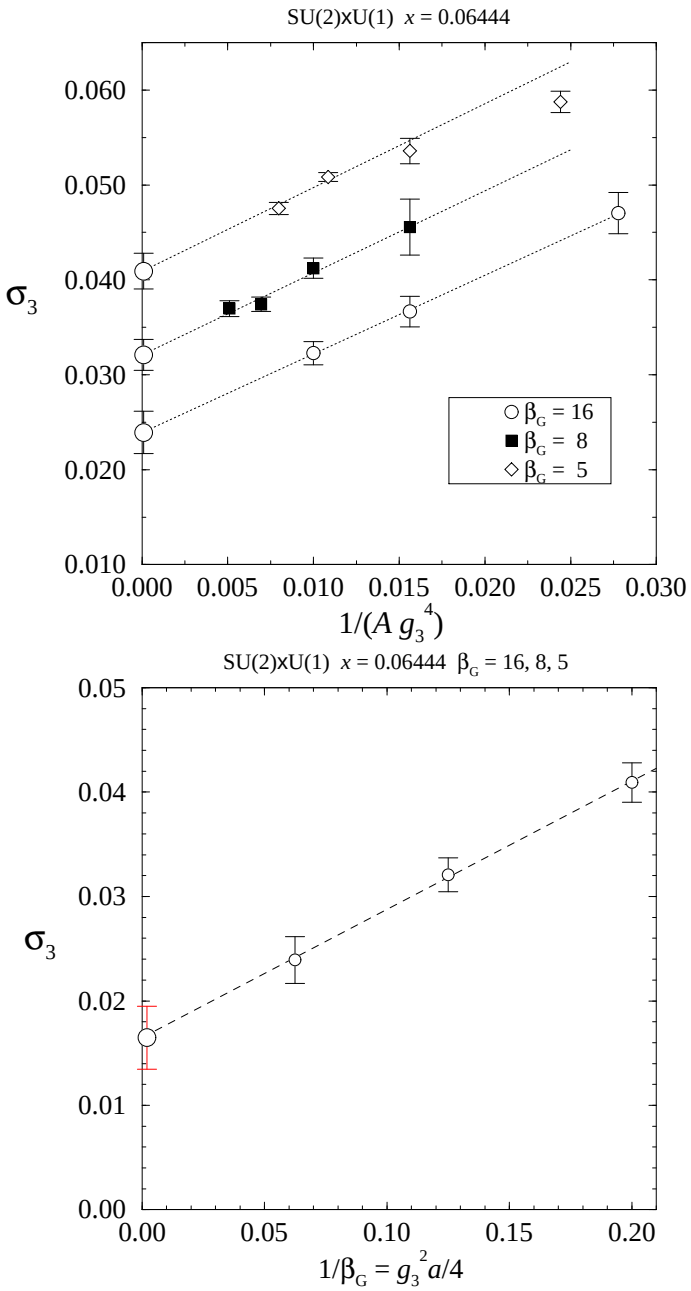

Figure 9: The interface tension σ_3 extrapolated to infinite volume (top) and then to the continuum limit (bottom) for $x = 0.06444$, $z = 0.3$.

volume with respect to $1/A$ (Fig. 10), and these values are in turn extrapolated to the continuum limit. The final results are shown in Table 3.

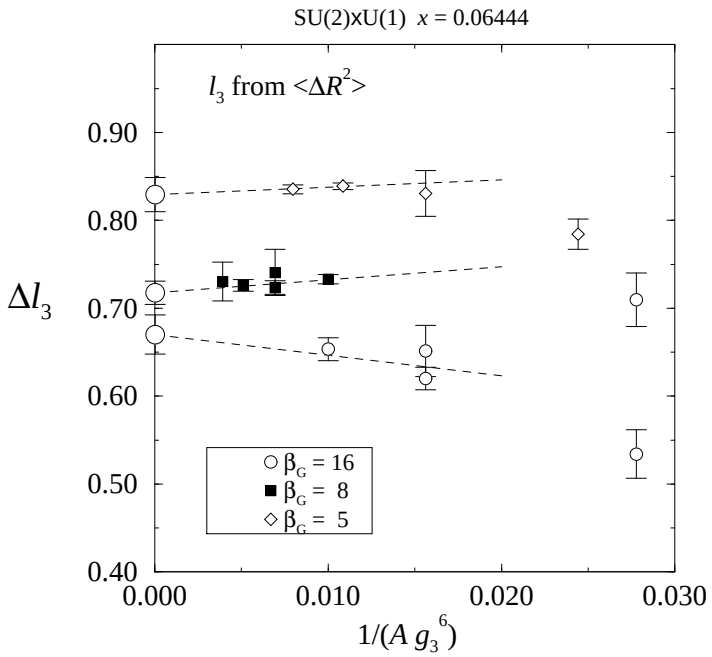

Figure 10: The infinite volume limit of the discontinuity $\Delta\langle\phi^\dagger\phi\rangle/g_3^2$ for $x = 0.06444$, $z = 0.3$. The extrapolation is done linearly in $1/A$, where A is the smallest cross-sectional area of the system.

An alternative method for calculating $\Delta\langle\phi^\dagger\phi\rangle$ is to use eq. (2.1) and measure

$$\frac{\Delta\langle\phi^\dagger\phi\rangle}{g_3^2} = \frac{-1}{Vg_3^6}\frac{d\Delta\log Z}{dy} = \frac{-1}{Vg_3^6}\frac{d\Delta P}{dy}, \tag{6.3}$$

where ΔP is the difference of the probabilities of the two phases and the derivatives are evaluated at the transition point (where $P_{\text{symm.}} = P_{\text{broken}} = 1/2$). The result obtained with this method is quite compatible with the above one.

6.3 Higgs and W correlators

We measure the masses of H and W^3 with the lattice versions of the operators $\phi^\dagger\phi$ and $\mathrm{Tr}\,\Phi^\dagger iD_i\Phi\sigma_3$, respectively. The correlation functions are measured in the direction of the x_3 -axis, and in order to enhance the projection to the ground states, we use blocking in the (x_1, x_2)-plane. The fields are recursively mapped from blocking level $(k) \to (k+1)$ ($\Phi^{(k)}(x) \to \Phi^{(k+1)}(y)$), so that the fields on the $(k+1)$-level lattice are in effect defined only on the even points of the (k)-level lattice on the (x_1, x_2)-plane, doubling the lattice spacing along the (x_1, x_2)-plane: $(a_1, a_2, a_3)^{(k+1)} = (2a_1, 2a_2, a_3)^{(k)}$.

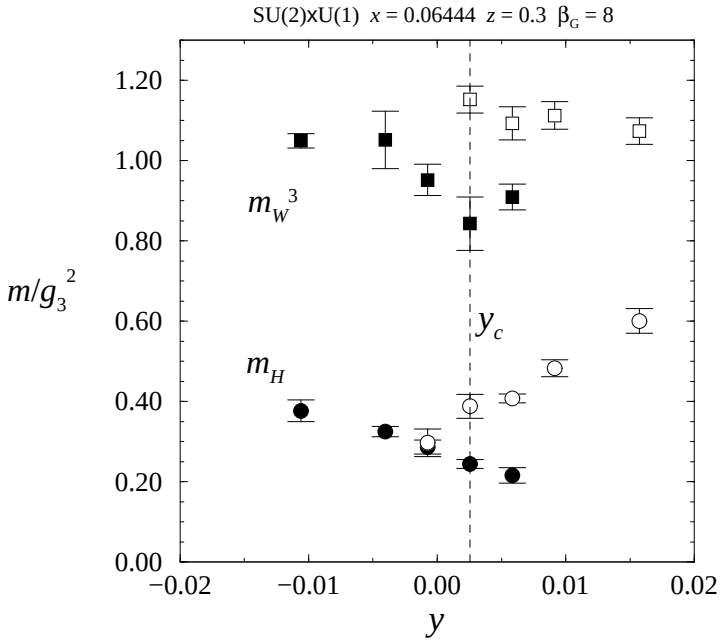

Figure 11: m_H and m_{W^3} measured from a $\beta_G = 8$, volume $= 32^2 \times 64$ -lattice. Filled symbols correspond to broken phase, open symbols to symmetric phase masses.

The blocking is performed with the transformations

$$\Phi^{(k+1)}(y) = \frac{1}{5}\Phi^{(k)}(x) + \frac{1}{5}\sum_{i=\pm 1,2} U_i^{(k)}(x)\Phi^{(k)}(x+i)\exp[-i\alpha_i^{(k)}(x)\sigma_3] \tag{6.4}$$

and $(i = 1, 2, j \neq i)$

$$\begin{aligned} U_i^{(k+1)}(y) &= U_i'^{(k)}(x)U_i'^{(k)}(x+i), & (6.5)\\ U_i'^{(k)}(x) &= \frac{1}{3}U_i^{(k)}(x) + \frac{1}{3}\sum_{j=\pm 1,2} U_j^{(k)}(x)U_i^{(k)}(x+j)U_j^{(k)\dagger}(x+i), & (6.6) \end{aligned}$$

where $(x_1, x_2, x_3) \equiv (2y_1, 2y_2, y_3)$ and $U_{-i}(x) = U_i^\dagger(x-i)$. The U(1) gauge field $B_i^{(k)} \equiv \exp[-i\alpha_i^{(k)}\sigma_3]$ is blocked with a transformation similar to (6.5–6.6). With the blocked fields we can define the operators

$$\begin{aligned} h^{(k)}(z) &= \sum_x \delta_{x_3,z}\mathrm{Tr}\,\Phi^{(k)\dagger}(x)\Phi^{(k)}(x), & (6.7)\\ w_i^{3(k)}(z) &= \sum_x \delta_{x_3,z}\mathrm{Tr}\,\Phi^{(k)\dagger}(x)U_i^{(k)}(x)\Phi^{(k)}(x+i)\exp[-i\alpha_i^{(k)}(x)\sigma_3]\sigma_3. & (6.8) \end{aligned}$$

These operators are used to calculate the zero transverse momentum correlation functions

$$H^{(k)}(l) = \frac{1}{V}\sum_z h^{(k)}(z)h^{(k)}(z+l), \tag{6.9}$$

$$W^{3(k)}(l) = \frac{1}{2V}\sum_{z;\,i=1,2} w_i^{3(k)}(z)w_i^{3(k)}(z+l), \tag{6.10}$$

and the masses are measured from the exponential fall-off in these functions. The blocking method used here resembles the one used by Philipsen et al. [8]; however, we do not perform the diagonalization of the full cross-correlation matrix formed of operators of different blocking levels.

For the Higgs channel the blocking makes little difference, and for the final results we use non-blocked ($k = 0$) operators. For W^3, on the other hand, the blocking improves the signal substantially, and we use 3 times blocked operators $W^{3(3)}$ to measure the W^3 mass. At $x = 0.06444$ we measure the masses using $\beta_G = 8$, $32^2 \times 64$ lattices and performing simulations on both sides of the transition. The metastability of the transition is large enough to permit the mass measurements also in the metastable branches, as shown in Fig. 11. This figure can be compared with the SU(2)+Higgs masses in Fig. 16 of [3]; it should be noted that there the y range $-0.066 < y < 0.042$ around the critical coupling y_c is much wider than in Fig. 11.

6.4 The photon screening mass

The qualitative difference between the SU(2)×U(1) theory considered in this paper and the SU(2)+Higgs model studied earlier is the presence of an extra gauge boson, associated with the U(1) group. This particle is massless in all orders of perturbation theory.

There are several questions which can be addressed here. The first one is associated with the very existence of the massless vector excitation. Indeed, there are known examples when the photon gets a mass due to some non-perturbative effects. For example, in compact (discretized) QED in three dimensions the photon in fact does not exist and is replaced by a massive pseudo-scalar excitation [24]. If some non-perturbative photon mass is generated, then, as has been argued in [25], the problem of the primordial magnetic monopoles would be solved.

The second question is associated with $Z-\gamma$ mixing. At sufficiently large and positive y (high temperatures) one would say that the massless excitation corresponds mainly to the hypercharge field B, while at large negative values of y (small temperatures) it is a mixture of the hypercharge field and the third component of the SU(2) gauge field. Since the SU(2)×U(1) theory does not contain a local gauge-invariant order parameter distinguishing the "broken" and "symmetric" phases, at sufficiently large values of the

parameter x (Higgs mass), the "content" of the hypercharge field in the massless state should interpolate smoothly between the two limiting cases.

Both questions can be studied non-perturbatively on the lattice. In order to have a sensible plane-plane correlation function, we define the operator [26]

$$O_{\mathbf{p}}(z) = \sum_{x_1,x_2} [\mathrm{Im}\, u_{12}(x_1, x_2, z)] \exp(i\mathbf{p}\cdot\mathbf{x}), \tag{6.11}$$

where the sum is taken over the plane (x_1, x_2), u_{ij} is the plaquette corresponding to the abelian U(1)-field, and $\mathbf{p}$ is a transverse momentum vector restricted to plane $(1, 2)$: $(p_1, p_2, p_3) = 2\pi/N(n_1, n_2, 0)$ with integer n_i (there is quantization of the momentum because of the periodic boundary conditions). In the continuum limit the operator O is just

$$O_{\mathbf{p}}(z) = \frac{1}{\sqrt{a\beta'_G}} \int dx_1 dx_2 B_{12}(x_1, x_2, z) \exp(i\mathbf{p}\cdot\mathbf{x}) \tag{6.12}$$

Note that if $\mathbf{p} = 0$, eq. (6.12) becomes identically zero in the absence of the winding modes.

The correlator of two plane operators,

$$G(z) = \frac{1}{N^3} \langle \sum_t O_{\mathbf{p}}(t) O^*_{\mathbf{p}}(z + t) \rangle \tag{6.13}$$

has the long-distance behaviour

$$G(z) = \frac{A_\gamma}{2\beta'_G} \frac{ap^2}{\sqrt{p^2 + m_\gamma^2}} \exp(-z\sqrt{p^2 + m_\gamma^2}), \tag{6.14}$$

where m_γ is the photon mass and A_γ is measuring the projection of the lowest mass state to the hypercharge U(1) field. In the tree approximation we have $A_\gamma = 1$ in the "symmetric" phase and $A_\gamma = \cos^2\theta_W$ in the "broken" phase. For simplicity, eq. (6.14) is written in terms of the continuum dispersion relation instead of the lattice one; due to the small values of $\mathbf{p}$ used here the effect the effect of the different dispersion relations is well below the statistical errors in this analysis. As one can see, the use of a momentum dependent operator in (6.11) is essential for a non-zero result for the correlation function.

In the simulations we used the two smallest possible transverse momenta, $\mathbf{p} = 2\pi/N\, \mathbf{e_i}$, with $i = 1$ or 2. In Fig. 12 we show the photon correlation function, measured from a $x = 0.62402$, $\beta_G = 8$ -system; all other parameter values yield very similar correlation functions. The results are perfectly consistent with the existence of the massless vector state. Applying eq. (6.14), the individual fits yield randomly positive or negative values for m_γ^2 (compatible with zero within the statistical errors); as a final result we give an upper bound for the photon mass over the whole parameter range:

$$m_\gamma \lesssim 0.03 g_3^2. \tag{6.15}$$

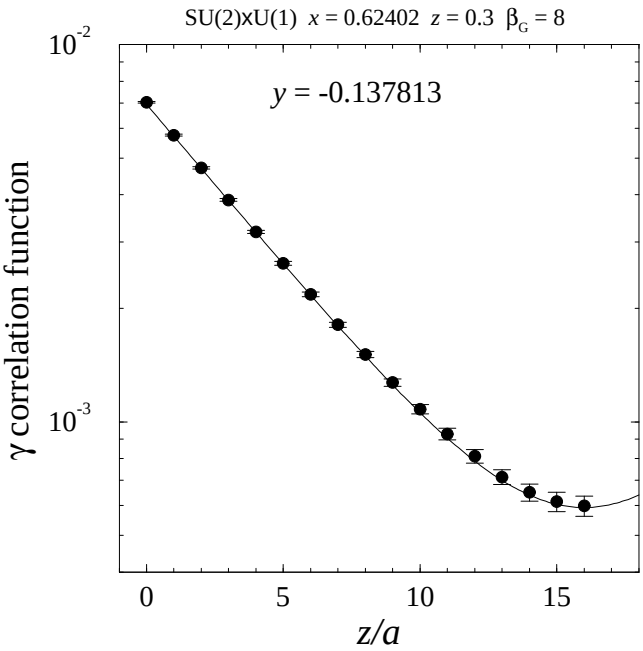

Figure 12: The photon correlation function eq. (6.14) for $x = 0.62402$ at the cross-over value for y, for a lattice of size 32^3. The continuous line is a 2-parameter fit to the distance range 4–16.

As to the mixing parameter A_γ, in the vicinity of the phase transition with $x = 0.06444$ we observe a sharp discontinuity in accordance with expectations (see Fig. 13). Note that here the discontinuity in A_γ is considerably smaller than given by the tree-level formula. This can to some extent be understood perturbatively; indeed, it is relatively easy to calculate at 1-loop order the residy of the $1/k^2$ pole in the U(1) correlator $\langle B_i B_j \rangle$ (this determines A_γ through (6.12)–(6.14)). In the symmetric phase ($m_3^2 > 0$), one gets

$$A_\gamma^{\rm symm} = 1 - \frac{g_3'^2}{48\pi m_3} = 1 - \frac{z}{48\pi\sqrt{y}}, \tag{6.16}$$

whereas in the broken phase the result is

$$A_\gamma^{\rm broken} = \cos^2\theta_W \Big(1 + \frac{11}{12} \frac{e_3^2}{\pi m_W} \Big), \tag{6.17}$$

where $e_3^2 = g_3^2 \sin^2\theta_W = g_3^2 g_3'^2/(g_3^2 + g_3'^2)$ and m_W is the perturbative W mass. It can be verified that these expressions are gauge-independent. Both corrections have the right sign and even roughly the right magnitude. In the symmetric phase, the expansion breaks down close to the transition point as $y \sim 0$.

As one approaches the endpoint of the line of the first order transitions, the discontinuity of A_γ gets smaller (together with m_W). When $x = 0.62402$ (which is safely above

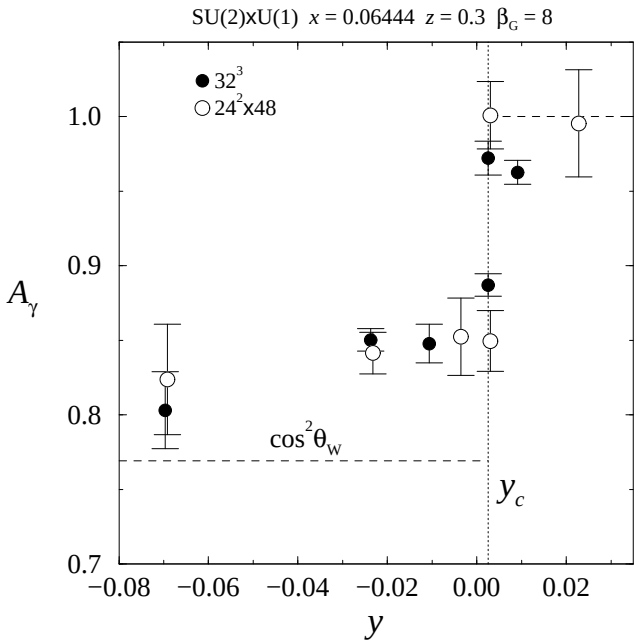

Figure 13: The pre-exponential factor A_γ for the $x = 0.06444$ case. The dashed horizontal lines are the tree-level values for A_γ in the symmetric and broken phases.

the endpoint) we observe a continuous change in the mixing parameter $A_\gamma \sim 1$ across the cross-over region. Thus, our non-perturbative analysis confirms within statistical errors the existence of the massless state which follows from perturbation theory, and demonstrates the absence of jumps of the mixing parameter in the region of large Higgs masses.

6.5 Absence of spontaneous parity breaking

A priori, it is not excluded that the Euclidean 3d non-abelian gauge-Higgs system exhibit spontaneous parity breaking in the strongly coupled phase. Arguments in favour of this possibility, based on the computation in [27] of the renormalization of the 3d topological mass term, were given in [28]. Lattice simulations in the symmetric phase of the SU(2)+Higgs system were carried out in [29], where no signal for spontaneous parity breaking was found. Here we extend the analysis of [29] to the more realistic SU(2)×U(1) case.

Consider some local gauge invariant operator O which is odd under the parity transformation. If there is spontaneous parity breaking in the system, the probability distribution of the quantity

$$\frac{1}{V}\int d^3x\, O(x), \tag{6.18}$$

where the integral is taken over a finite volume V, must have a double-peak structure, which becomes more pronounced when the volume of the system increases. Simultaneously, the susceptibility defined as

$$\chi(V,T) = \int d^3x \langle O(x)O(0)\rangle, \tag{6.19}$$

must behave as $\chi(V,T_c) \propto V^1$ when $V \to \infty$. If spontaneous parity breaking is absent, the probability distribution of O looks like a single peak with center at zero, and $\chi(V,T_c) \propto V^0$.

Our choice of parity breaking operators includes the the lattice versions of the operators (2.15–2.16) and the operator

$$W_P(x) = \epsilon_{ijk} W_i^3(x) W_j^+(x) W_k^-(x), \tag{6.20}$$

where $W^\pm \equiv W^1 \pm iW^2$. The study of the non-local operators (2.17) corresponding to the Chern-Simons numbers, was not attempted because it would be very time consuming.

We found that the expectation values of all of these operators remain consistent with zero in both symmetric and broken phases at $x = 0.06444$ near the phase transition. More precisely, the distribution of the operators is very accurately Gaussian centered around zero; moreover, the autocorrelations of the successive measurements are negligible even in the transition region, where all of the other measurements show significant autocorrelations. This implies that the parity operators decouple from the long-distance dynamics and are sensitive only to the local ultraviolet noise of the system. The susceptibility χ was found to be practically volume independent for all of the volumes, again signifying the non-critical nature of the parity operators. The situation is similar at $x = 0.62402$ in the cross-over region. Thus, the possibility of non-perturbative parity breaking is ruled out (at least within the statistical accuracy and for the volumes used in our simulations) for the SU(2)×U(1) theory as well.

6.6 The transition in the $x = 0.62402$ case

When $x = 0.62402$ (in [4] this value of x corresponds to $m_H^* = 180\,\mathrm{GeV}$) and $z = 0.3$ the transition has turned into a smooth and regular cross-over, completely analogously to the SU(2)+Higgs $z = 0$ case. This can be observed, for example, by monitoring the behaviour of the order parameter susceptibility and the correlation lengths. For example, in Fig. 14 we show the behaviour of the $\phi^\dagger\phi$ susceptibility χ_ϕ as a function of y for several volumes; in the case of a true transition the susceptibility diverges at the transition point ($\propto V$ for a first order transition, $\propto V^\gamma$ for a second order one). In this case no divergence is seen, only a volume independent smooth peak corresponding to the cross-over behaviour. For this x we have data only for $\beta_G = 8$, and using the

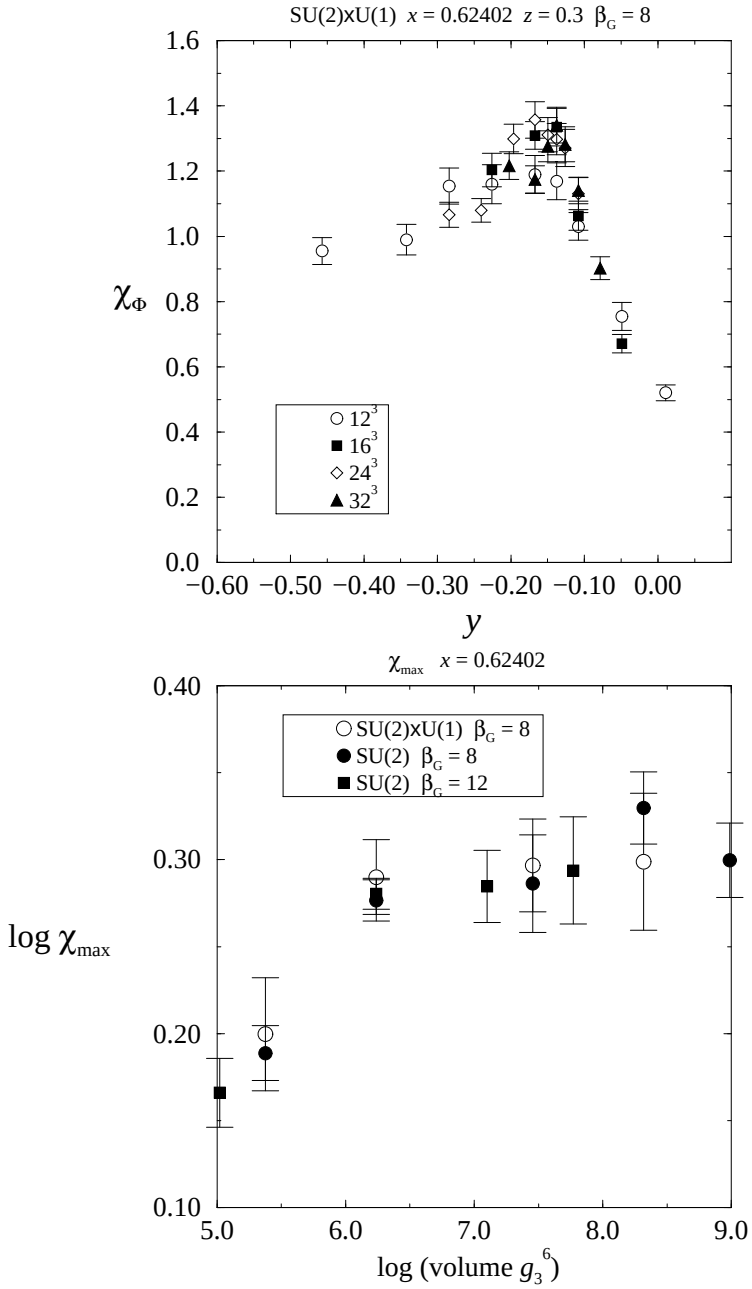

Figure 14: The $\phi^\dagger\phi$ susceptibility χ_ϕ measured from $\beta_G = 8$, $x = 0.62402$ lattices as a function of y. No divergence develops when the volume increases (top). The maximum values of the susceptibility χ_ϕ as a function of the volume for SU(2)+Higgs and SU(2)×U(1)+Higgs systems (bottom).

maximum location of χ_ϕ we extrapolate the infinite volume cross-over coupling to be $y_c(x = 0.62402, z = 0.3, \beta_G = 8) = -0.152(7)$.

In Fig. 14 we compare the maximum values of χ_ϕ for SU(2)+Higgs and SU(2)×U(1)+

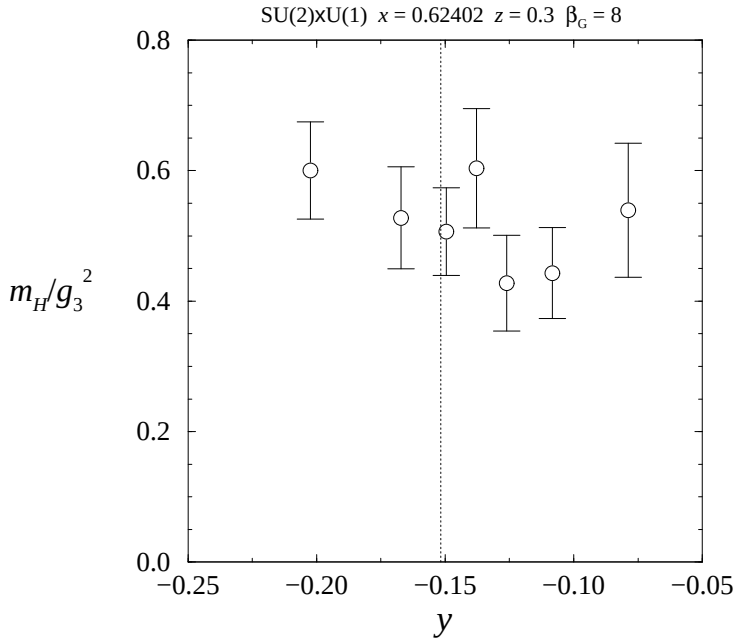

Figure 15: The scalar correlation length from a $\beta_G = 8$, $x = 0.62402$, volume $= 32^3$ lattice as a function of y. The dotted line shows the location of the maximum of χ_ϕ.

Higgs theories at $x = 0.62402$; the SU(2)+Higgs data is from [4]. The quantitative behaviour of the systems is quite similar, and there is no first order transition. In Fig. 15 we show the (lightest) scalar mass across the transition region; it remains non-zero as in the SU(2)+Higgs, signalling the absence of a second order transition. The photon mass vanishes everywhere in both phases (see Sec. 6.4), and hence it should not affect the order of the transition.

7 Conclusions

We have in this paper studied numerically the 3d SU(2)×U(1)+fundamental Higgs theory and compared it with the 3d SU(2)+fundamental Higgs theory at the same values of the coupling $x = \lambda_3/g_3^2$, but for $g_3'^2 \neq 0$. The comparison has been made both in a region with a clear first-order transition ($x = 0.06444; m_H^* = 60$ GeV) and in the cross-over region ($x = 0.62402; m_H^* = 180$ GeV). The main conclusion is that the inclusion of U(1) does not bring in significant new non-perturbative effects: the changes in the non-perturbatively computed quantities due to increasing $g_3'^2$ are as large as those given by perturbation theory. At the same time, the values of the observables themselves, especially σ_3, differ from those in perturbation theory. In particular, the first order transition ends at some x_c as in 3d SU(2)+Higgs and for $x > x_c$ there is

no first or second order transition. A still higher order transition cannot be strictly excluded by the analysis presented in this paper.

We have also confirmed non-perturbatively the existence of a (nearly) massless photon in the 3d SU(2)×U(1)+Higgs model. We have studied the mixing of this state to the Lagrangian U(1)-field, and demonstrated that the jump in the mixing parameter vanishes together with the first order transition as one goes to large enough Higgs masses. Physically these results on the photon imply that magnetic fields are not screened in hot electroweak plasma even taking into account all nonperturbative effects.

Acknowledgements

M.L was partially supported by the University of Helsinki.

References

[1] K. Kajantie, M. Laine, K. Rummukainen and M. Shaposhnikov, Nucl. Phys. B 458 (1996) 90 [hep-ph/9508379].

[2] J.M. Cline and K. Kainulainen, Nucl. Phys. B, in press [hep-ph/9605235]; M. Losada, hep-ph/9605266; M. Laine, Nucl. Phys. B 481 (1996) 43 [hep-ph/9605283].

[3] K. Kajantie, M. Laine, K. Rummukainen and M. Shaposhnikov, Nucl. Phys. B 466 (1996) 189 [hep-lat/9510020].

[4] K. Kajantie, M. Laine, K. Rummukainen and M. Shaposhnikov, Phys. Rev. Lett. 77 (1996) 2887 [hep-ph/9605288].

[5] K. Kajantie, K. Rummukainen and M. Shaposhnikov, Nucl. Phys. B 407 (1993) 356; K. Farakos, K. Kajantie, K. Rummukainen and M. Shaposhnikov, Phys. Lett. B 336 (1994) 494; Nucl. Phys. B 442 (1995) 317 [hep-lat/9412091].

[6] E.-M. Ilgenfritz, J. Kripfganz, H. Perlt and A. Schiller, Phys. Lett. B 356 (1995) 561 [hep-lat/9506023]; M. Gürtler, E.-M. Ilgenfritz, J. Kripfganz, H. Perlt and A. Schiller, hep-lat/9512022; hep-lat/9605042.

[7] F. Karsch, T. Neuhaus, A. Patkós and J. Rank, Nucl. Phys. B 474 (1996) 217 [hep-lat/9603004].

[8] O. Philipsen, M. Teper and H. Wittig, Nucl. Phys. B 469 (1996) 445 [hep-lat/9602006].

[9] F. Csikor, Z. Fodor, J. Hein, K. Jansen, A. Jaster and I. Montvay, Phys. Lett. B 334 (1994) 405; Z. Fodor, J. Hein, K. Jansen, A. Jaster and I. Montvay, Nucl. Phys. B 439 (1995) 147; F. Csikor, Z. Fodor, J. Hein and J. Heitger, Phys. Lett. B 357 (1995) 156; F. Csikor, Z. Fodor, J. Hein, A. Jaster and I. Montvay, Nucl. Phys. B 474 (1996) 421.

[10] K. Rummukainen, Proceedings of Lat96, Nucl. Phys. B (Proc. Suppl.).

[11] A. Jakovác, K. Kajantie and A. Patkós, Phys. Rev. D 49 (1994) 6810; A. Jakovác and A. Patkós, Phys. Lett. B 334 (1994) 391.

[12] T. Banks and E. Rabinovici, Nucl. Phys. B 160 (1979) 349.

[13] E. Fradkin and S.H. Shenker, Phys. Rev. D 19 (1979) 3682.

[14] J. Fröhlich, G. Morchio and F. Strocchi, Nucl. Phys. B 190 (1981) 553.

[15] V. Matveev, A. Tavkhelidze and M. Shaposhnikov, Teor. i mat. fizika 59 (1984) 328.

[16] M. Laine, Nucl. Phys. B 451 (1995) 484 [hep-lat/9504001].

[17] G.D. Moore, PUPT-1649 [hep-lat/9610013].

[18] K. Farakos, K. Kajantie, K. Rummukainen and M. Shaposhnikov, Nucl. Phys. B 425 (1994) 67 [hep-ph/9404201].

[19] P. Arnold and O. Espinosa, Phys. Rev. D 47 (1993) 3546; Phys. Rev. D 50 (1994) 6662 (E).

[20] Z. Fodor and A. Hebecker, Nucl. Phys. B 432 (1994) 127.

[21] A.M. Ferrenberg and R.H. Swendsen, Phys. Rev. Lett. 61 (1988) 2635.

[22] A. Berg and T. Neuhaus, Phys. Lett. B 267 (1991) 267.

[23] K. Binder, Phys. Rev. A 25 (1982) 1699.

[24] A.M. Polyakov, Nucl. Phys. B 120 (1977) 429.

[25] A.D. Linde, Phys. Lett. B 96 (1980) 293.

[26] B. Berg and C. Panagiotakopoulos, Phys. Rev. Lett. 52 (1984) 94; H.G. Evertz, K. Jansen, J. Jersák, C.B. Lang and T. Neuhaus, Nucl. Phys. B 285 (1987) 590.

[27] R.D. Pisarski and S. Rao, Phys. Rev. D 32 (1985) 2081.

[28] S.Yu. Khlebnikov and M.E. Shaposhnikov, Phys. Lett. B 254 (1991) 148.

[29] J. Ambjørn, K. Farakos and M.E. Shaposhnikov, Mod. Phys. Lett. A 6 (1991) 3099; Nucl. Phys. B 393 (1993) 633.